Applied Catalysis B: Environmental 152–153 (2014) 46–50

Contents lists available at ScienceDirect

Applied Catalysis B: Environmental

journal homepage: www.elsevier.com/locate/apcatb

Fabrication of atomic single layer graphitic-C_3N_4 and its high performance of photocatalytic disinfection under visible light irradiation

Huanxin Zhao, Hongtao Yu, Xie Quan*, Shuo Chen, Yaobin Zhang, Huimin Zhao, Hua Wang

Key Laboratory of Industrial Ecology and Environment Engineering (Ministry of Education, China), School of Environmental Science and Technology, Dalian University of Technology, Dalian 116024, China

ARTICLE INFO

Article history:
Received 6 November 2013
Received in revised form 6 January 2014
Accepted 13 January 2014
Available online 22 January 2014

Keywords:
Single layer
g-C_3N_4
Photocatalytic disinfection
Metal free
Visible light

ABSTRACT

Photocatalytic disinfection over a high performance metal-free photocatalyst under visible light irradiation was studied. An atomic single layer g-C_3N_4 (SL g-C_3N_4) with the thickness of 0.5 nm was fabricated by a two-step approach including thermal etching of bulk g-C_3N_4 into g-C_3N_4 nanosheets (g-C_3N_4 NS) and followed by an ultrasonic exfoliation of g-C_3N_4 NS. The performance of photocatalytic disinfection was investigated by inactivation of *Escherichia coli*. Under the visible light irradiation, 2×10^7 cfu mL^{-1} of *E. coli* could be killed completely over the SL g-C_3N_4 within 4 h, whereas only about 3 log and 5 log of *E. coli* could be killed on bulk g-C_3N_4 and g-C_3N_4 NS under the same condition, respectively. Especially, the direct destruction of the *E. coli* cell wall was observed by TEM. The enhancement of photocatalytic efficiency of SL g-C_3N_4 was attributed to the low charge transfer resistance and efficient charge separation which were confirmed by electrochemical impedance spectroscopy and photo-current measurements. Owing to the excellent performance of SL g-C_3N_4, a visible light response and environmental friendly photocatalyst for disinfection was achieved.

1. Introduction

The removal of pathogenic microorganisms from water is quite important for the human health. Although traditional disinfection technologies such as chlorination and ozonation were highly effective for inactivation, they usually produce harmful disinfection by-products with carcinogenic and mutagenic potential [1]. UV disinfection is recognized as a "green" technology without any chemical agent [2], however some microorganisms are highly resistant to UV radiation and the regrowth occurs after 72–96 h [3,4]. Since photocatalytic inactivation with TiO_2 reported by Matsunaga et al. for the first time [5], semiconductor heterogeneous photocatalysis is considered as a promising alternative way for disinfection. However, the most widely used TiO_2 photocatalyst is only active under UV irradiation. From the viewpoint of utilizing solar light, developing visible light response photocatalyst for disinfection is more significant since 45% of the sunlight spectrum is visible light.

Recently, several visible light driven photocatalysts such as Ag doped TiO_2 [6–8], AgX (X is Br, I and S) [9–11], $CdIn_2S_4$ and $ZnIn_2S_4$ [12,13] have been proposed to disinfection. Nevertheless, these photocatalysts suffer from the ever-present release of heavy metal ions which is potential harmful to human health. For example, the leakage of Ag^+ were 0.27 and 0.55 mg L^{-1} from Ag/AgBr/TiO_2 and AgBr–Ag–Bi_2WO_6 reported by Hou and Zhang, respectively [14,15], which were beyond the US EPA (Environmental Protection Agency) drinking water standard of 0.1 mg L^{-1}. For the $CdIn_2S_4$ [12], the elution of Cd^{2+} was as high as 0.2 mg L^{-1}, 40 times of US EPA drinking water standard. Therefore, developing high performance and safe photocatalyst based on a metal-free material for disinfection under visible light irradiation is desired.

Wang and coworkers synthetized the graphene and graphitic-C_3N_4 (g-C_3N_4) nanosheets co-wrapped elemental α-sulfur as a metal-free photocatalyst for bacterial inactivation [16]. However the component and the fabrication procedure are complicated. Therefore, a simpler component and higher efficiency photocatalyst is still expected. As a metal-free photocatalyt, g-C_3N_4 has attracted much attention both in H_2 production [17–19] and contaminants degradation [20,21]. However the photocatalytic efficiency of pristine g-C_3N_4 is still rather low due to the fast recombination of photo-generated charges. Exfoliating the bulk g-C_3N_4 into g-C_3N_4 nanosheets (g-C_3N_4 NS, with thickness of 2–3 nm,) is an efficient pathway to improve its photocatalytic performance [22,23]. Meanwhile, the theoretical calculation indicated that the

* Corresponding author. Tel.: +86 411 84706263; fax: +86 411 84706263.
E-mail address: quanxie@dlut.edu.cn (X. Quan).

0926-3373/$ – see front matter © 2014 Elsevier B.V. All rights reserved.
http://dx.doi.org/10.1016/j.apcatb.2014.01.023

emergence of optical and electronic properties would facilitate the photocatalysis when the thickness of g-C_3N_4 reached to atomic single layer [24]. It is expected that the single layer g-C_3N_4 (SL g-C_3N_4) will exhibit better performance than g-C_3N_4 NS for photocatalytsis [25,26].

Here we report for the first time the fabrication of SL g-C_3N_4 for application in photocatalytic disinfection under visible light irradiation. It is shown that the photocatalytic efficiency of SL g-C_3N_4 significantly improved due to the efficient photo-generated charge separation. Moreover, to study the photocatalytic mechanism of disinfection, chemical scavengers were used to interact with different active species. The stability of the as-prepared SL g-C_3N_4 was also investigated.

2. Experimental

2.1. Materials

The fabrication procedure of bulk g-C_3N_4 can be found in our previous work [27]. In detail, 5 g of melamine was calcined at 520 °C for 4 h with the heating rate of 5 °C min^{-1}. After calcination, the received bulk g-C_3N_4 was milled into powder and heated at 550 °C for 3 h to prepare the g-C_3N_4 NS. At last, 10 mg of the obtained g-C_3N_4 NS was dispersed in 100 mL isopropanol at room temperature and exfoliated by ultrasonication for 8 h. The final product was centrifuged and dried in vacuum at 50 °C for 6 h.

2.2. Characterization

The morphologies of the samples were characterized by field emission scanning electron microscope (FE-SEM S4800 Hitach), transmission electron microscopy (TEM Tecnai G^2 S-Twin) and atomic force microscopy (AFM Agilent PicoPlus). The crystal face structures were characterized by X-ray diffractometer (Shimadzu Lab-X XRD-6000). The chemical structure information was investigated by Fourier transform spectrophotometer (FT-IR, VERTEX 70, Bruker) with KBr as the reference sample.

2.3. Photoelectrochemical measurements

The photocurrent and Nyquist plots were measured using an electrochemical station (CHI660D, Shanghai Chenhua Limited, China) in a conventional three-electrode configuration with the working electrode, a platinum sheet as the counter electrode and a saturation calomel electrode (SCE) as the reference electrode. To fabricate working electrodes for conducting the photoelectrochemical measurements, the ethanol dispersion of samples ca. 0.25 mg mL^{-1} was uniformly spin-dropped on the indium tin oxide (ITO)-coated glass at 7500 rpm by a desktop spin coater (TC 100 spin coater MTI Corporation China) firstly. Then the ITO glass with liquid film was held at 300 °C for 120 min to volatilize the ethanol. The electrolyte was 0.01 M Na_2SO_4 aqueous solution. The light source was a high pressure xenon short arc lamp (CHF-XM35-150W, Beijing Changtuo Co.), whose light intensity was 100 mW cm^{-2}.

2.4. Photocatalytic disinfection of Escherichia coli

E. coli was incubated in Luria Bertani nutrient solution at 37 °C for 12 h with shaking and then washed with 0.9% saline. After centrifugation, the cell was re-suspended with 0.9% saline. The experiments of photocatalytic disinfection were carried out by using a 500 W Xe lamp. The light was passed through a UV cut-off filter ($\lambda > 400$ nm), and then was focused onto a flask containing a suspension of bacterial cells and photocatalyst. The final photocatalyst concentration and cell density were adjusted to 0.1 g L^{-1} and about 2×10^7 colony forming units per milliliter (cfu mL^{-1}), respectively. At the certain time intervals, 1 mL of suspension was sampled and immediately diluted 10-fold serially with sterilized saline. In order to measure the density of viable *E. coli* cell, 0.2 mL of the diluted solution was spread on the nutrient agar and incubated at 37 °C for 12 h. The number of cfu was counted to determine the number of viable cells. Each set of experiment was performed in triplicate and their average values with statistical deviation were used in the data analysis. The glassware was autoclaved at 121 °C for 20 min to ensure sterility. The scavenger experiments were carried out by adding individual scavenger to the photocatalytic reaction system. KI, isopropanol and Cr(VI) were used to remove h^+, •OH and e^-, respectively [28].

2.5. Preparation of E. coli for TEM

At given time intervals, the cell suspension was collected and centrifuged down to pellets. The bacteria pellets were prefixed by 2.5% glutaraldehyde and trapped in 3% low melting point agarose. After being postfixed by 1% osmium tetraoxide (E.M. grade, Electron Microscopy Sciences, Fort Washington, PA, USA) in phosphate buffer (0.1 M, pH 7.2), the cell pellet was dehydrated by adding a graded series of ethanol and finally embedded in Spurr solution (Electron Microscopy Sciences, Fort Washington, PA, USA) for polymerization at 68 °C. An ultramicrotome (Leica, Reichert Ultracuts, Wien, Austria) was used to make ultrathin sections of 70 nm and stain with uranyl acetate and lead citrate on copper grids. Finally, the stained ultrathin sections were examined by a TEM [29].

3. Results and discussion

3.1. Characterization of photocatalysts

Fig. 1(a) shows the SEM image of the product after ultrasonic exfoliation. Many flakes with laminar morphology were observed. In contrast, the bulk g-C_3N_4 without exfoliation was composed with irregular particles (Fig. S1). The HRTEM image of the product after ultrasonic exfoliation as presented in Fig. 1(b) displayed layer structure with some chiffon-like ripples and wrinkles. To further

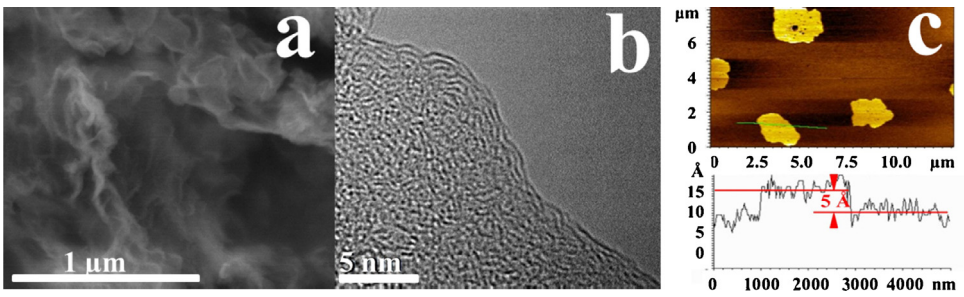

Fig. 1. Morphology of the SL g-C_3N_4: (a) SEM image; (b) TEM image; (c) AFM image.

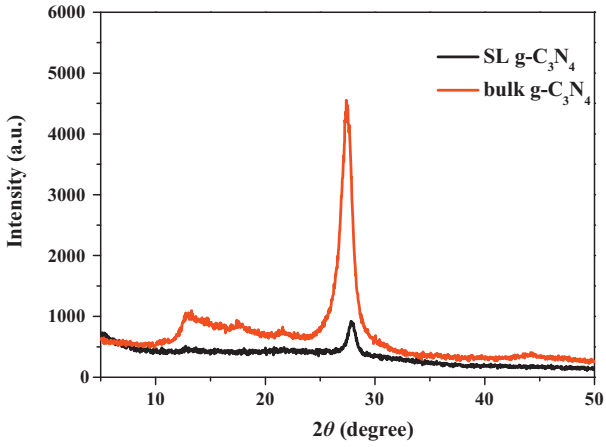

Fig. 2. XRD patterns of bulk g-C_3N_4 and SL g-C_3N_4.

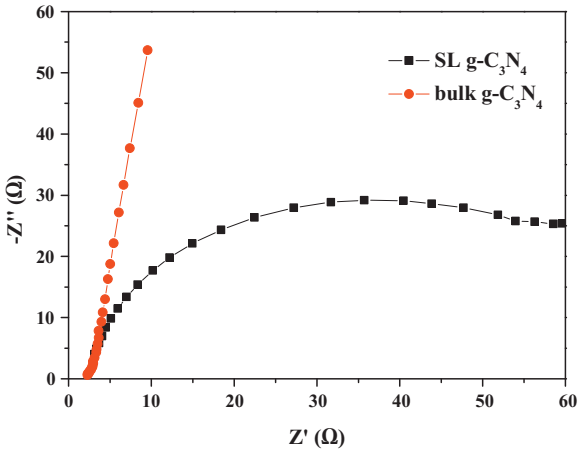

Fig. 4. EIS spectra of bulk g-C_3N_4 and SL g-C_3N_4.

understand the thickness of the product before and after the ultrasonic exfoliation, AFM measurement was carried out. The thickness of g-C_3N_4 NS before ultrasonic treatment was around 2.5 nm (Fig. S2), which was consistent with the literature for the few layer g-C_3N_4 nanosheets [22]. After ultrasonic exfoliation, the SL g-C_3N_4 was successfully fabricated (Fig. 1(c)) and the thickness of the sample was only 0.5 nm. This value of the thickness was as same as that of graphene reported for the first time [30]. In detail, this thickness contents the interlayer distance (0.326 nm) in bulk g-C_3N_4 and a "dead layer" between the sample and the SiO_2 substrate owing to the adsorbed water [30].

XRD analysis was carried out to investigate the crystal structure of the samples. As Fig. 2 shown, two characteristic peaks of bulk g-C_3N_4 could be observed. One is the strong peak at 27.5° corresponding to the (0 0 2) plane, which is attributed to the interlayer distance d = 0.326 nm in bulk g-C_3N_4. The other is the week peak at 13.1° corresponding to the (100) plane, which is related to the in-plane structural packing motif of tri-*s*-triazine units. For the SL g-C_3N_4, the peak at 27.5° got much weaker, which indicated the interlayer structure was destroyed after exfoliation. Meanwhile, the chemical structures of the samples were further analyzed by FTIR and the results were showed in Fig. 3. The board peaks between 3000 and 3500 cm^{-1} corresponded to the N–H band. The peaks at 1251, 1325, 1419, 1571, and 1639 cm^{-1} were contributed to the typical stretching modes of CN heterocycles. In addition, the characteristic breathing mode of triazine units at 810 cm^{-1} is observed [31]. It is worth noting that there were no differences of FTIR peak between bulk g-C_3N_4 and the SL g-C_3N_4, which indicated that the chemical structure of SL g-C_3N_4 was as same as that of bulk g-C_3N_4.

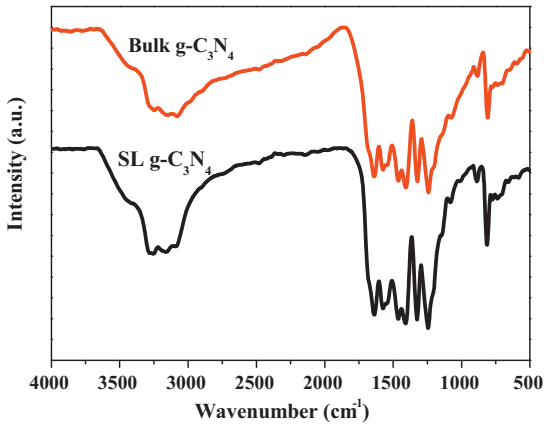

Fig. 3. FTIR spectra of bulk g-C_3N_4 and SL g-C_3N_4.

3.2. Efficient photo-generated charge separation

Photo-generated charge separation is a crucial factor during the photocatalytic process. Obviously, the atomic single layer structure of g-C_3N_4 could shorten the transfer distance for photo-generated charges arriving to the surface which decrease the probability of the recombination. Additionally, according to the diffusion formula of $t = d^2/(k^2D)$ (d is the particle size, k is a constant, D is the diffusion coefficient of electron–hole pairs) [32], the ultrathin thickness and two-dimensional conducting channels of SL g-C_3N_4 help it to achieve low charge-transfer resistance [33]. Verified by the corresponding EIS which is a powerful tool to clarify the charge-transport resistance (Fig. 4), it is observed that the semicircle in the plot got shorter for the SL g-C_3N_4 than bulk g-C_3N_4. This result indicated a decrease of charge–transfer resistance on the surface of SL g-C_3N_4 [34]. The short transfer distance and the low charge-transfer resistance promote the photo-generated charge separate efficiently and react with target immediately, thus the enhancement of photocatalytic efficiency is expected. Photocurrent measurements were also carried out to evaluate the capacity of photogenerated charge separation. The SL g-C_3N_4 displayed a much enhanced photocurrent density of 1.8 μA cm^{-2}, about 17 times that of bulk g-C_3N_4 (Fig. 5).

3.3. Photocatalytic disinfection performance and the mechanism

E. coli as a common pathogenic microorganism were chosen as a representative microorganism to evaluate the photocatalytic

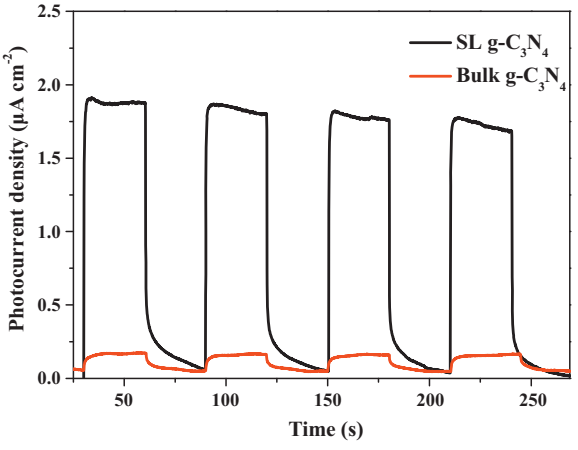

Fig. 5. Photocurrent–time dependence of bulk g-C_3N_4 and SL g-C_3N_4 electrodes under visible light irradiation (λ > 400 nm).

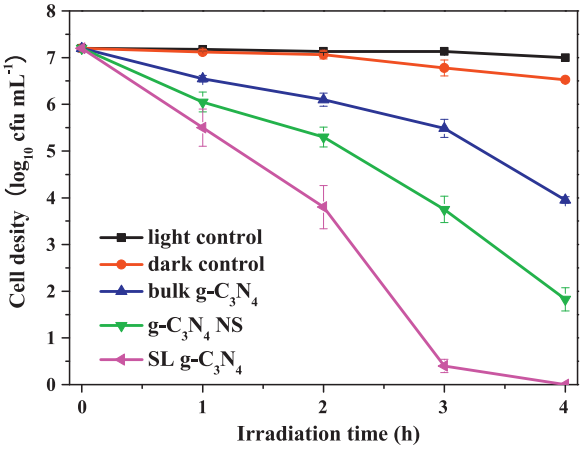

Fig. 6. Photocatalytic disinfection efficiencies under different conditions.

disinfection performance. Fig. 6 shows the photocatalytic disinfection efficiencies of *E. coli* over different photocatalysts. The cell density is nearly unchanged in dark (dark control) which indicated no toxic effect of SL g-C_3N_4 to *E. coli* cell. Also when the photocatalyst was absent (light control), no *E. coli* was killed which confirmed that the cell could not be destroyed by visible light irradiation. With the visible light irradiation on SL g-C_3N_4, 2×10^7 cfu mL^{-1} of *E. coli* could be killed completely in 4 h, whereas only ~3 log and 5 log of *E. coli* could be killed over bulk g-C_3N_4 and g-C_3N_4 NS under the same condition, respectively. Compared with the bulk g-C_3N_4 and g-C_3N_4 NS, the SL g-C_3N_4 exhibited the best photocatalytic inactivation efficiency.

As well known, h^+, •OH and e^- are often proposed to be the reactive oxidative species responsible for the photocatalytic disinfection. To understand which reactive species played an important role in SL g-C_3N_4 photocatalytic disinfection under visible light irradiation, a series of scavenger experiments were carried out by adding individual scavenger to the photocatalytic reaction system. In our experiments, 5 mM KI, 0.5 mM isopropanol and 0.05 mM Cr(VI) were used to remove h^+, •OH and e^-, respectively. As reported, all the scavengers had no toxic effect on *E. coli* at this level of concentrations [35]. As shown in Fig. 7, with the addition of isopropanol or Cr(VI), ~5 log of *E. coli* could be killed in 4 h. However, only ~2 log of *E. coli* could be killed with the addition of KI. These results indicated that SL g-C_3N_4 photocatalytic disinfection is the h^+ oxidation dominated process under visible light irradiation.

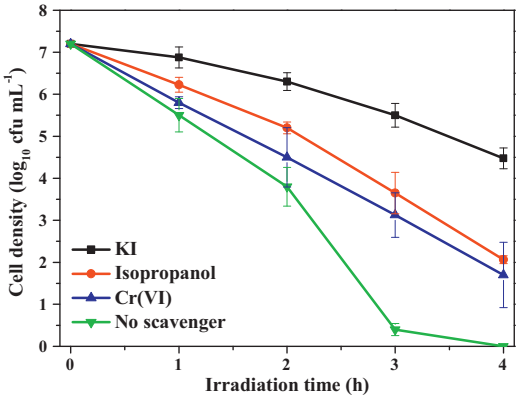

Fig. 7. Photocatalytic disinfection efficiencies of SL g-C_3N_4 with different scavengers.

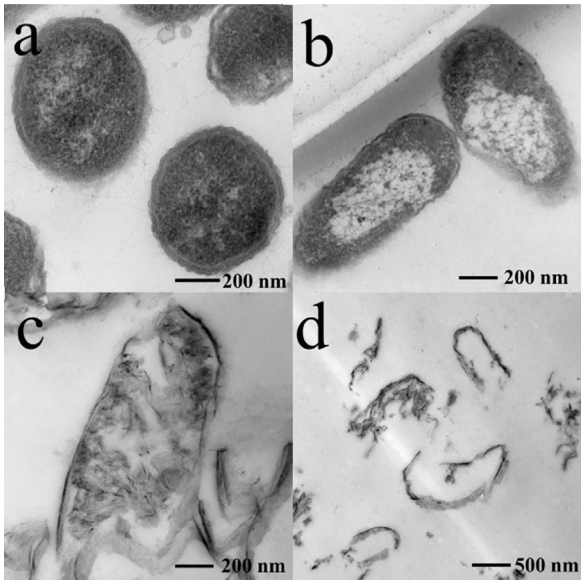

Fig. 8. TEM images of *E. coli* before and after photocatalytic disinfection. (a) Before irradiation, and after irradiated for (b) 4 h; (c) 8 h; (d) 12 h.

3.4. Destruction of E. coli cell and the stability of the SL g-C_3N_4

To further confirm the destruction of the *E. coli* cell, the morphology and microstructure of the *E. coli* before and after photocatalytic disinfection were examined by TEM. Fig. 8(a) shows a representative TEM image of *E. coli* before photocatalytic disinfection. A well-preserved cell wall could be observed. After 4 h irradiation (Fig. 8(b)), clearly, the cell wall was partly damaged. An electron translucent region was observed at the center of the cell indicating the leakage of the interior component. After 8 h irradiation (Fig. 8(c)), the cell wall was seriously damaged and the whole cell was almost transparent under the electron beam. After irradiation for 12 h (Fig. 8(d)), only a small portion of the cell debris was left indicating a complete destruction of bacterial cell.

The stability of SL g-C_3N_4 was investigated by successive cycle of photocatalytic disinfection of *E. coli* experiments and the result was showed in Fig. 9. Clearly, the SL g-C_3N_4 did not exhibit any significant loss of activity on photocatalytic disinfection even after three cycles of repeated experiments indicating that the SL g-C_3N_4 is stable in the disinfection process.

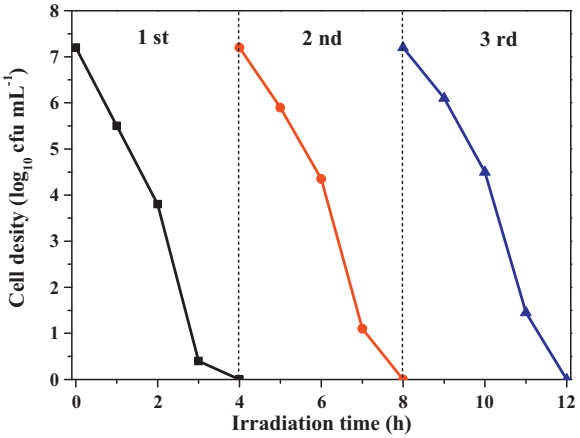

Fig. 9. Stability of SL g-C_3N_4 under visible light irradiation.

4. Conclusion

In summary, we highlight an available pathway to photocatalytic disinfection under visible light irradiation over an atomic single layer g-C_3N_4. A simple metal-free and high performance technology of disinfection was achieved. The enhancement of photocatalytic efficiency was attributed to the efficient photogenerated charge separation owing to the single layer structure. The application of SL g-C_3N_4 on photocatalytic disinfection will facilitate development of safe and reliable disinfection technology.

Acknowledgments

This work was supported by National Basic Research Program of China (2011CB936002) and National Natural Science Foundation of China (No. 21077018).

Appendix A. Supplementary data

Supplementary data associated with this article can be found, in the online version, at http://dx.doi.org/10.1016/j.apcatb.2014.01.023.

References

[1] M.G. Muellner, E.D. Wagner, K. McCalla, S.D. Richardson, Y.-T. Woo, M.J. Plewa, Environ. Sci. Technol. 41 (2007) 645–651.
[2] L. Liberti, M. Notarnicola, G. Boghetich, A. Lopez, Aqua 50 (2001) 275–285.
[3] Y. Gilboa, E. Friedler, Water Res. 42 (2008) 1043–1050.
[4] M.V. Yates, J. Malley, P. Rochelle, R. Hoffman, J. Am. Water Works Assoc. 98 (2006) 93–106.
[5] T. Matsunaga, R. Tomoda, T. Nakajima, H. Wake, FEMS Microbiol. Lett. 29 (1985) 211–214.
[6] L. Liu, Z. Liu, H. Bai, D.D. Sun, Water Res. 46 (2012) 1101–1112.
[7] P. Wu, R. Xie, K. Imlay, J.K. Shang, Environ. Sci. Technol. 44 (2010) 6992–6997.
[8] Z. Xiong, J. Ma, W.J. Ng, T.D. Waite, X.S. Zhao, Water Res. 45 (2011) 2095–2103.
[9] M.R. Elahifard, S. Rahimnejad, S. Haghighi, M.R. Gholami, J. Am. Chem. Soc. 129 (2007) 9552–9553.
[10] X. Hu, C. Hu, T. Peng, X. Zhou, J. Qu, Environ. Sci. Technol. 44 (2010) 7058–7062.
[11] M. Pang, J. Hu, H.C. Zeng, J. Am. Chem. Soc. 132 (2010) 10771–10785.
[12] W. Wang, T.W. Ng, W.K. Ho, J. Huang, S. Liang, T. An, G. Li, J.C. Yu, P.K. Wong, Appl. Catal., B 129 (2013) 482–490.
[13] H. Yu, X. Quan, Y. Zhang, N. Ma, S. Chen, H. Zhao, Langmuir 24 (2008) 7599–7604.
[14] Y. Hou, X. Li, Q. Zhao, G. Chen, C.L. Rastor, Environ. Sci. Technol. 46 (2012) 4042–4050.
[15] L.-S. Zhang, K.-H. Wong, H.-Y. Yip, C. Hu, J.C. Yu, C.-Y. Chan, P.-K. Wong, Environ. Sci. Technol. 44 (2010) 1392–1398.
[16] W. Wang, J.C. Yu, D. Xia, P.K. Wong, Y. Li, Environ. Sci. Technol. 47 (2013) 8724–8732.
[17] X. Wang, S. Blechert, M. Antonietti, ACS Catal. 2 (2012) 1596–1606.
[18] X. Wang, K. Maeda, X. Chen, K. Takanabe, K. Domen, Y. Hou, X. Fu, J. Am. Chem. Soc. 131 (2009) 1680–1681.
[19] X. Wang, K. Maeda, A. Thomas, K. Takanabe, G. Xin, J.M. Carlsson, K. Domen, M. Antonietti, Nat. Mater. 8 (2009) 76–80.
[20] Y. Cui, J. Huang, X. Fu, X. Wang, Catal. Sci. Technol. 2 (2012) 1396–1402.
[21] S.C. Yan, Z.S. Li, Z.G. Zou, Langmuir 26 (2010) 3894–3901.
[22] P. Niu, L. Zhang, G. Liu, H.-M. Cheng, Adv. Funct. Mater. 22 (2012) 4763–4770.
[23] S. Yang, Y. Gong, J. Zhang, L. Zhan, L. Ma, Z. Fang, R. Vajtai, X. Wang, P.M. Ajayan, Adv. Mater. 25 (2013) 2452–2456.
[24] X. Zhang, X. Xie, H. Wang, J. Zhang, B. Pan, Y. Xie, J. Am. Chem. Soc. 135 (2013) 18–21.
[25] J. Xu, L. Zhang, R. Shi, Y. Zhu, J. Mater. Chem. A1 (2013) 14766–14772.
[26] H. Zhao, H. Yu, X. Quan, S. Chen, H. Zhao, H. Wang, RSC Adv. 4 (2014) 624–628.
[27] G. Liao, S. Chen, X. Quan, H. Yu, H. Zhao, J. Mater. Chem. 22 (2012) 2721–2726.
[28] Y. Chen, A. Lu, Y. Li, L. Zhang, H.Y. Yip, H. Zhao, T. An, P.K. Wong, Environ. Sci. Technol. 45 (2011) 5689–5695.
[29] S. Pigeot-Rémy, F. Simonet, E. Errazuriz-Cerda, J.C. Lazzaroni, D. Atlan, C. Guillard, Appl. Catal., B 104 (2011) 390–398.
[30] K.S. Novoselov, A.K. Geim, S.V. Morozov, D. Jiang, Y. Zhang, S.V. Dubonos, I.V. Grigorieva, A.A. Firsov, Science 306 (2004) 666–669.
[31] A. Thomas, A. Fischer, F. Goettmann, M. Antonietti, J.-O. Mueller, R. Schloegl, J.M. Carlsson, J. Mater. Chem. 18 (2008) 4893–4908.
[32] R.I. Bickley, T. GonzalezCarreno, L. Palmisano, R.J.D. Tilley, J.M. Williams, Mater. Chem. Phys. 51 (1997) 47–53.
[33] Y. Sun, Z. Sun, S. Gao, H. Cheng, Q. Liu, J. Piao, T. Yao, C. Wu, S. Hu, S. Wei, Y. Xie, Nat. Commun. 3 (2012) 1057–1063.
[34] W.H. Leng, Z. Zhang, J.Q. Zhang, C.N. Cao, J. Phys. Chem. B 109 (2005) 15008–15023.
[35] W. Wang, Y. Yu, T. An, G. Li, H.Y. Yip, J.C. Yu, P.K. Wong, Environ. Sci. Technol. 46 (2012) 4599–4606.